Available online at www.eccomasproceedia.org
Eccomas Proceedia COMPDYN (2017) 2181-2202

ECCOMAS
Proceedia

COMPDYN 2017
6th ECCOMAS Thematic Conference on
Computational Methods in Structural Dynamics and Earthquake Engineering
M. Papadrakakis, M. Fragiadakis (eds.)
Rhodes Island, Greece, 15–17 June 2017

SEISMIC RESPONSE OF A HIGH-PIER BRIDGE SUBJECTED TO OBLIQUE INCIDENCE WAVES

Yin Gu[1], Hongxiang Guo[1] and Weidong Zhuo[1]

[1] Fuzhou University
academy road no. 2, new district of Fuzhou University, Fuzhou city, Fujian province
cinoa@fzu.edu.cn, Guohxfzu@163.com, zhouwd@fzu.edu.cn

Keywords: Seismic Analysis, High-Pier Bridge, Oblique Incidence Waves, Viscous-Spring Artificial Boundary, Soil-Structure Dynamic Interaction, P Wave, SV Wave

Abstract. *Oblique incidence waves play a vital role in the spatial variation of seismic ground motions. It is important to consider the oblique incidence of a seismic wave in a valley or in other complex topographies. It is too expensive for realistic 3D simulations of a soil-bridge system. In the work reported here, an efficient method of artificial boundary has been substantially improved, and the numerical simulation method of free field with uniform topographic under oblique incidence waves is studied. The numerical accuracy is tested by comparing with the analytical solutions. A finite element model of a bridge-soil system is built to analyze the seismic response of a continuous rigid-frame bridge with high piers located in a plain topography as well as deep valley with the consideration of oblique incidence waves. The topographic effect on amplitude and distribution of internal forces were determined for different oblique incident angles and different shear wave velocities of the soil. The dynamic response of this bridge under P-wave and SV-wave are summarized. The results show that the angle of the oblique incidence waves has greater effect on internal forces of the piers and piles in a deep valley than in uniform field shapes. If the bridge is located in a valley, the effect of oblique incidence waves on the bridge should be considered.*

Peer-review under responsibility of the organizing committee of COMPDYN 2017.
doi: 10.7712/120117.5559.17335

1. ITRODUCTION

The non-uniform effects of long-span bridges under spatial variations of ground motions cannot be neglected. The oblique incidence of the waves is one of the most important spatial effects. Based on common models, earthquakes are mainly expected to be shear waves propagating vertically. However, in near fields, the seismic waves have oblique incidence with spatial distributions characters. It means that there are different amplitudes and durations at different locations of the structure. Two directions, including horizontal and vertical directions, coupled together have great effect on the soil-structure dynamic interaction system. In recent years, there have been many studies for seismic response considering oblique incidence waves. But most of the studies concern the analysis of underground soil-structure systems, which include subway stations and buried pipes. The studies have shown that the response of the underground structure under oblique incidence waves is different from those under vertical wave only. The structure is not safe by neglecting the oblique incidence waves under this condition[Du *et al*., 2007, Wang *et al*., 2008, Chen *et al*., 2007, Alys *et al*., 1992]. Bonganoff *et al*. [1965]found that the non-uniform excitation is significantly different in various types of structures. The time-lag effect in seismic wave propagation has an influence on a large-span structure. The spatial distribution in seismic field was first considered in the European code [EN, 1995]. The spatial distribution has also been included in seismic analysis of large-span bridges in the Chinese code [JTG/TB 02-01-2008, 2008].

It is a reasonable assumption that a small structure on a plain topography subjected to a uniform seismic wave is used in the analysis of a soil-structure dynamic interaction numerical model. Topography can cause scattering and diffraction of incoming seismic waves, and can result in amplifications and de-amplifications of earthquake ground motions [Trifunac. 1973, Zhang *et al*., 2012]. The seismic wave propagation will be difficult to calculate owing to the complex topography, which has great effects on bridges with high piers, especially those with quite varied pier heights or long spans. This problem brought concerns to researchers[Liu *et al*., 2011, Zhou. 1992]that the seismic ground motion is obviously different in a valley than in the plain. These differences and their spatial effects should be considered. [Liu, 2005] studied the seismic response of bridges under oblique incidence and the topographic effect. The results show that the response of the structure is larger in comparison with the traditional consideration of the vertical wave. So the effect of oblique incidence waves on the bridge should be considered for complex topographic.

Many earlier studies have numerically modeled seismic wave scatter around a single canyon or hill mainly in order to compare the results of numerical approaches with an analytical or semi-analytical solution[Gaffet and Bouchon, 1989]. Rayleigh method is proposed for investigating the amplification by surface topographic irregularities in reference[Paolucci, 2002]. A hybrid FD-FE (Finite difference and Finite element) method for interaction between topographic irregularities and seismic ground motion was also explored[Ariane and Mideo, 2012]. Also, some authors have applied numerical methods to study wave propagation in more complex real cases. However, few systematic studies have been conducted to analyze the interaction between structure and the typical topography with oblique incidence waves.

In spite of all the studies above, it is still complicated to consider how to input earthquake waves, especially oblique incidence waves, directly on the soil-structure system. We present a procedure for how to conduct a simple finite element analysis(FEA) model considering soil-structure interaction and how to input the seismic waves with oblique incidence in finite element analysis. The method used in several case studies to show the effect of the topography and the angle of the oblique incidence waves on bridges.

2. EQUIVALENT ARTIFICIAL BOUNDARY ELEMENT

The finite element method is widely used in numerical analysis considering local non-regular topography. Studies shows that the damping ratio of the structure-soil system increases by 25% compared with a model with spring and dampers. The latter model responds differently from the more accurate former system [Zhang *et al*. 2001, Sun *et al*. 2002]. In the structure-soil system the limited computing area should be cut from the unlimited earth medium. An artificial boundary is added to the boundary to simulate the radiation damping of a continuous medium. It should be verified that the radial waves do not reflect back to the limited computing area. The numerical approaches that have been developed include absorbing boundaries, the Boundary Element Method, infinite elements， the thin-layer method, perfectly matched layers and the scaled boundary FEM (SBFEM). Extensive reviews of most of these methods are available and not repeated here[Gu, 2007].

Absorbing boundaries including the global artificial boundary usually possess high accuracy and good robustness, but are complicated and computationally expensive. The local artificial boundary, viscous boundary, proposed by Lysmer and Kulemeyer [1969], is known as the differential artificial boundary condition. The movement of a boundary joint is just dependent on the adjacent points. Owing to its simplicity and good applicability, the viscous boundary has been applied widely in wave problems. [Deeks, 1994] established a 2D artificial boundary in the time domain based on the cylinder wave theory. Based on it, [Liu, 2005]introduced the viscous-spring artificial boundary in 2D, and derived a 3D viscous-spring artificial boundary using the spherical wave theory. The viscous-spring artificial boundary has the stiffness parameters to consider the elastic recovery. It is better than the viscous boundary, which are not stable in low frequency. The model with this boundary can simulate the radiation damping and elastic resumption behavior of the semi-infinite medium.

As stated above, lots of artificial boundary methods have been proposed. Most of the methods are complicated and not easy for engineering applications. It is an acceptable method to add forces on nodes with the equivalent force based on the concept of a viscous-elastic artificial boundary. Based on the theory of a viscous-spring artificial boundary, a simple method to solve the soil-structure dynamic problem and meet the engineering precision is proposed here. An equivalent viscous-spring artificial boundary element is developed in this section for building the simple model of the soil-structure dynamic interaction system.

2.1 Development of equivalent artificial boundary element

The 3D viscous-spring artificial boundary equations were deduced by the spherical wave theory. In the spherical surface $r=R$, the normal stresses in the medium are given in terms of the displacement by

$$\sigma_r + \frac{R}{c_p}\dot{\sigma}_r = -\frac{4\mu}{R}\left[u + \frac{R}{c_p}\dot{u} + \frac{\rho R^2}{4\mu}\ddot{u}\right] \tag{1}$$

The 3D artificial boundary equations in tangential direction have the form

$$\tau(R,t) = -\frac{2G}{R}u(R,t) - \rho c_s \dot{u}(R,t) \tag{2}$$

According to the wave propagation equation in spherical coordinate, the boundaries are equivalent to a series of distributed springs and dampers system in three directions[Li, 2005]. According to the numerical adjustment, the coefficient deduced from the total space can be changed to a half space problem. In the 3D system, using the variables α_T and α_N, the elastic stiffness coefficient K and the damping coefficient C can be represented as

$$K_{BT} = {}_T\frac{G}{R}, \quad C_{BT} = c_s \tag{3}$$

$$K_{BN} = {}_N\frac{G}{R}, \quad C_{BN} = c_p \tag{4}$$

where K_{BT} and C_{BT} are tangential stiffness and damping coefficient, respectively; K_{BN} and C_{BN} are normal stiffness and damping coefficient, respectively. R represents the distance between the wave source and the artificial boundary, c_s and c_p represent the velocity of the shear wave and the compression wave in the soil, respectively, G is the shear modulus, ρ represents the mass density, α_N is coefficients range from 1 to 2.0, and α_T is coefficient range from 0.5 to 1. The recommended value of α_N is 1.33 and α_T is 0.67[Gu, 2005].

The dynamic soil-structure system with the viscous-spring boundary is shown in Fig. 1.

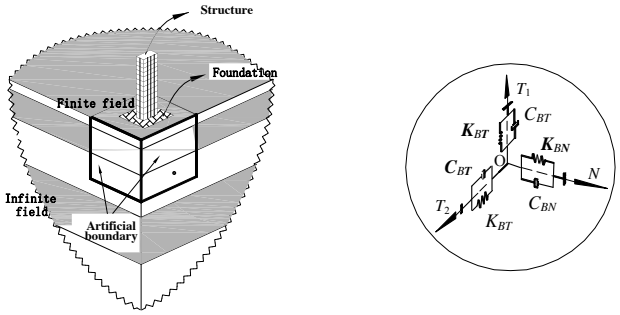

Fig. 1. Equivalent spring-damper system on artificial boundary

It is not convenience that the spring-damper system needs to be added on every node of the boundary surface of the large 3D soil-structure model. An equivalent artificial boundary element proposed here is to extend a layer of elements with the same type of inside elements along the normal direction. This equivalent solid element replaces the springs and dampers system as the boundary element. The outside boundaries of the artificial boundary element are fixed.

The replacement rule is based on the theory that both methods, spring-damper system and equivalent element, have the same stiffness. A simple solid finite element with eight nodes and six surfaces has been applied to simulate the 3D consistent artificial boundary. The solid element is shown in Fig. 2.

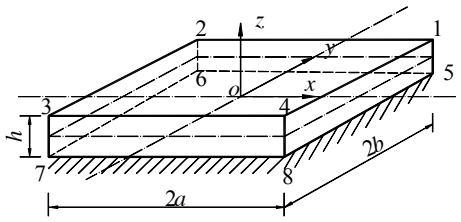

Fig.2. The hexahedral element

According to the shape function and the formula of matrix *K*

$$[K] = \int [B]^T [D][B] d\Omega \tag{5}$$

The stiffness matrix of element about node 1 is

$$[\tilde{K}]_{3d\_n1}=\begin{bmatrix} \frac{2}{9}(\frac{ah}{2b}g+\frac{2ab}{h}g+\frac{bh}{2a}m) & \frac{1}{12}hn+\frac{1}{12}hg & \frac{1}{12}bn-\frac{1}{12}bg \\ & \frac{2}{9}(\frac{ah}{2b}g+\frac{2ab}{h}g+\frac{bh}{a}m) & \frac{1}{12}an+\frac{1}{12}ag \\ & & \frac{2}{9}(\frac{ah}{2b}g+\frac{2ab}{h}m+\frac{bh}{2a}g) \end{bmatrix} \quad (6)$$

Where $m=E\dfrac{1\quad v}{(1+v)(1\quad v)}$, $n=E\dfrac{v}{(1+v)(1\quad v)}$, g =G。

when h approaches zero, the matrix about nodes 1,2,3,4 is close to

$$[\tilde{K}]_{3d}=\frac{ab}{9h}\begin{bmatrix} 4g & 0 & 0 & 2g & 0 & 0 & g & 0 & 0 & 2g & 0 & 0 \\ & 4g & 0 & 0 & 2g & 0 & 0 & g & 0 & 0 & 2g & 0 \\ & & 4m & 0 & 0 & 2m & 0 & 0 & m & 0 & 0 & 2m \\ & & & 4g & 0 & 0 & 2g & 0 & 0 & g & 0 & 0 \\ & & & & 4g & 0 & 0 & 2g & 0 & 0 & g & 0 \\ & & & & & 4m & 0 & 0 & 2m & 0 & 0 & m \\ & & & & & & 4g & 0 & 0 & 2g & 0 & 0 \\ & & & & & & & 4g & 0 & 0 & 2g & 0 \\ & & & & & & & & 4m & 0 & 0 & 2m \\ & & & & & & & & & 4g & 0 & 0 \\ & & & & & & & & & & 4g & 0 \\ & & & & & & & & & & & 4m \end{bmatrix} \quad (7)$$

The element stiffness matrix $[K]_{B\text{-}3d}$ of the consistent viscous-spring artificial boundary can be formed by integral operation too, which can be derived as

$$[K]_{B-3d}=\begin{bmatrix} \frac{4ab}{9}K_{BT} & 0 & 0 & \frac{2ab}{9}K_{BT} & 0 & 0 & \frac{ab}{9}K_{BT} & 0 & 0 & \frac{2ab}{9}K_{BT} & 0 & 0 \\ & \frac{4ab}{9}K_{BT} & 0 & 0 & \frac{2ab}{9}K_{BT} & 0 & 0 & \frac{ab}{9}K_{BT} & 0 & 0 & \frac{2ab}{9}K_{BT} & 0 \\ & & \frac{4ab}{9}K_{BN} & 0 & 0 & \frac{2ab}{9}K_{BN} & 0 & 0 & \frac{ab}{9}K_{BN} & 0 & 0 & \frac{2ab}{9}K_{BN} \\ & & & \frac{4ab}{9}K_{BT} & 0 & 0 & \frac{2ab}{9}K_{BT} & 0 & 0 & \frac{ab}{9}K_{BT} & 0 & 0 \\ & & \text{对称} & & \frac{4ab}{9}K_{BT} & 0 & 0 & \frac{2ab}{9}K_{BT} & 0 & 0 & \frac{ab}{9}K_{BT} & 0 \\ & & & & & \frac{4ab}{9}K_{BN} & 0 & 0 & \frac{2ab}{9}K_{BN} & 0 & 0 & \frac{ab}{9}K_{BN} \\ & & & & & & \frac{4ab}{9}K_{BT} & 0 & 0 & \frac{2ab}{9}K_{BT} & 0 & 0 \\ & & & & & & & \frac{4ab}{9}K_{BT} & 0 & 0 & \frac{2ab}{9}K_{BT} & 0 \\ & & & & & & & & \frac{4ab}{9}K_{BN} & 0 & 0 & \frac{2ab}{9}K_{BT} \\ & & & & & & & & & \frac{4ab}{9}K_{BT} & 0 & 0 \\ & & & & & & & & & & \frac{4ab}{9}K_{BT} & 0 \\ & & & & & & & & & & & \frac{4ab}{9}K_{BN} \end{bmatrix} \quad (8)$$

Comparing Eq. (7) with Eq. (8), when $[K]_{b-3d}=[\tilde{K}]_{3d}$ is true, then

$$\begin{cases} \dfrac{ab}{h}g=2abK_{BT} \\ \dfrac{ab}{h}m=2abK_{BN} \end{cases} \quad (9)$$

Arranging Eq.(9), the equivalent shear modules and elastic modules of boundary elements are

$$\begin{cases} \tilde{G} = hK_{BT} = 2\alpha_T h\dfrac{G}{R} \\ \tilde{E} = 2\dfrac{(1+\tilde{\nu})(1-2\tilde{\nu})}{(1-\tilde{\nu})} hK_{BN} = 2\alpha_N h\dfrac{G}{R}\cdot\dfrac{(1+\tilde{\nu})(1-2\tilde{\nu})}{(1-\tilde{\nu})} \end{cases} \quad (10)$$

The damping matrix is

$$[C] = \eta[K] = \eta\int [B]^T [D][B]dA \quad (11)$$

In which

$$[\eta] = \begin{bmatrix} \eta_{BT} & 0 & 0 \\ 0 & \eta_{BT} & 0 \\ 0 & 0 & \eta_{BN} \end{bmatrix}$$

where η is damping coefficient, which is in proportion to the stiffness in tangential and normal directions, respectively.

The coefficient η_{BT} and η_{BN} are

$$\eta_{BT} = \frac{C_{BT}}{K_{BT}} = \frac{\rho c_s R}{\alpha_T G} \quad (12)$$

$$\eta_{BN} = \frac{C_{BN}}{K_{BN}} = \frac{\rho c_p R}{\alpha_N G} \quad (13)$$

Applying to most of FEM software, there is only one damping coefficient can be set. Defined by isotropy material property, the average coefficient $\tilde{\eta}$ is

$$\tilde{\eta} = \frac{\rho R}{3G}(2\frac{c_s}{\alpha_T} + \frac{c_p}{\alpha_N}) \quad (14)$$

where, R represents the distance between the wave source and the artificial boundary, C_s and C_p represent the respective velocities of the shear wave and the compression wave in the soil respectively, G represents the shear modulus, ρ is the mass density, while α_T and α_N are respective coefficients whose values are specified with K_{BT} and K_{BN} calculated in equation (1).

According to Equations (10) and (14), the parameters of the equivalent element, $\tilde{G}, \tilde{E}$ and $\tilde{\nu}$, are defined for the orthotropic materials. But for the isotropic material, owing to the property limitation, $\tilde{\nu}$ and $\tilde{E}$ are dependent and their values should meet the implicit relationship about

$$\tilde{E} = 2(1+\tilde{\nu})\tilde{G} \quad (15)$$

when

$$= {}_N / {}_T \quad (16)$$

Consider Eq.(10) , Eq.(15) and Eq.(16), the relationship of equivalent Poisson's ratio $\tilde{\nu}$ and α can be expressed as

$$\tilde{\nu} = \frac{\alpha - 2}{2(\alpha - 1)} \quad (17)$$

The relationship of $\tilde{\nu}$ and α is shown in Fig.3. As we can see, if α<2, $\tilde{\nu}$ is a negative value. It breaks the normal physical material limitation laws in finite element (Poisson's ratio should be in range between 0 and 0.5). In this case of α<2, we set

$$\tilde{\nu} = 0$$

Then, we obtain

$$\tilde{\nu} = \begin{cases} \dfrac{\alpha - 2}{2(\alpha - 1)} & \alpha \geq 2 \\ 0 & others \end{cases} \tag{18}$$

It is shown in Fig.4 that if there has a limitation condition $\alpha \geq 2$, the values of α_T and α_N are not equal to the values defined in Table 1. So we have studied the robustness of this equivalent artificial boundary.

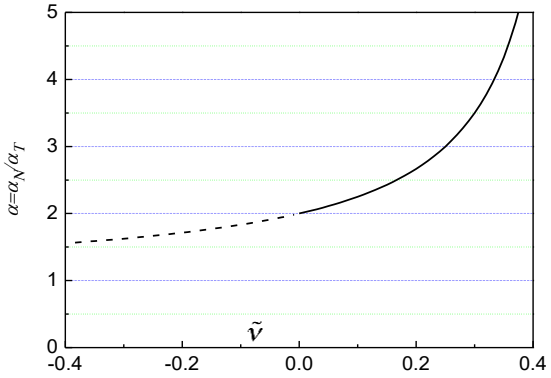

Fig. 3. Relationship of $\tilde{\nu}$ and α

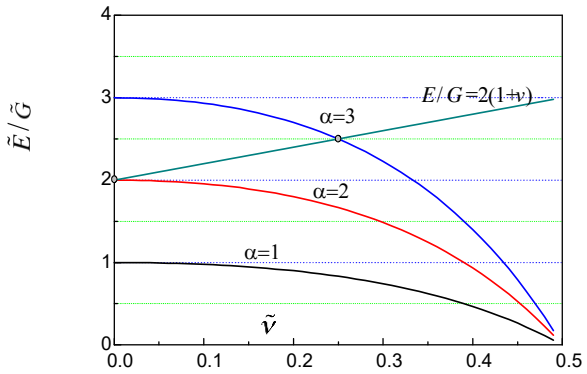

Fig. 4. Relationship of $\tilde{E}$, $\tilde{G}$ and $\tilde{\nu}$

2.2 Verification

Lamb problem The Lamb problem, which is also called the Dynamic Boussinesq problem, is chosen to verify the method above. The computational model of the Lamb problem is shown in Fig.5(a). This is a model with dimensionless form. The mass density of the solid is 1.The shear modulus is 16, and the Poisson ratio is 0.25. The 3D model size is 1×1×0.5. The time step is 0.01s. The loading function is described by δ function shown in Fig.5 (b) and the loading duration is 0.5s. In this example, α_T is chosen as 0.67, α_N as 1.33 and R as 0.5 and h=0.01. The equivalent artificial boundary is a solid element stretching from model with outer surface fixed.

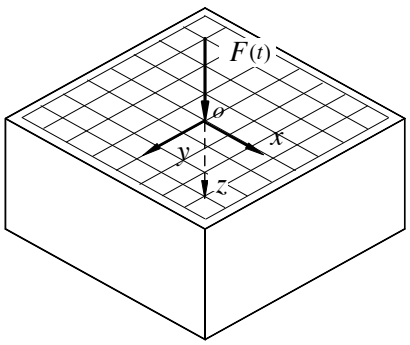

（a） The half space model with the 3D equivalent

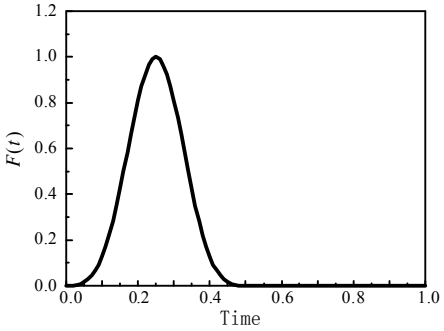

b）Loading function viscous-spring artificial boundary element

Fig.5. Lamb Problem

The time histories ofvertical displacements for one observation point on the model surface are shown in Fig.6. The curves include the analytic solution and the results computing with the viscous boundary, lump viscous-spring artificial boundary and the equivalent viscous-

spring artificial element boundary model. In Fig.6, the curve of consistent viscous-spring artificial boundary approaches to the lumped viscous-spring artificial boundary. Both curves are close to the theory solution. The consistent viscous-spring artificial boundary can be applied simply by using equivalent boundary element. Consider l=$2\sqrt{ab}$. The parameter h, which is proportion to the l, is changed to test the robust of the three-dimensional equivalent boundary element. The displacements of the observed points with different sizes of h are shown in Fig. 7. The relationship of parameters h, a and b is shown in Fig.2. r is distance from point of load.

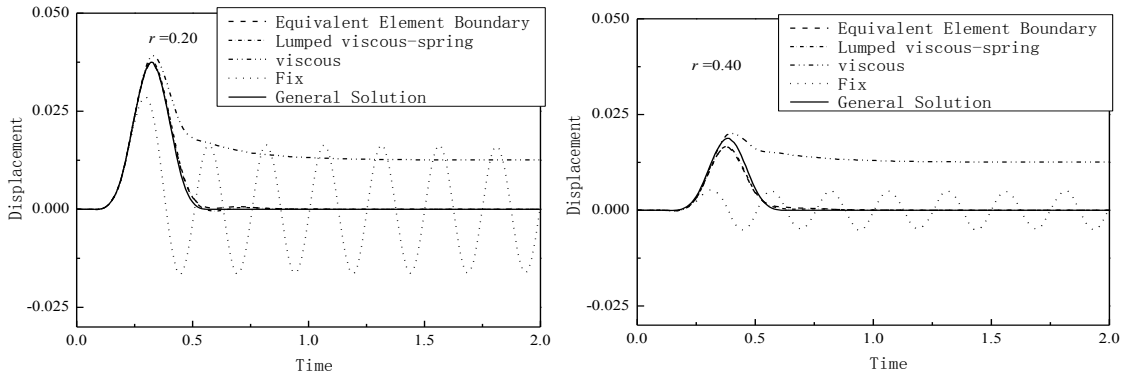

(a) r=0.20 (b) r=0.40

Fig. 6. The time history for displacements of observe point

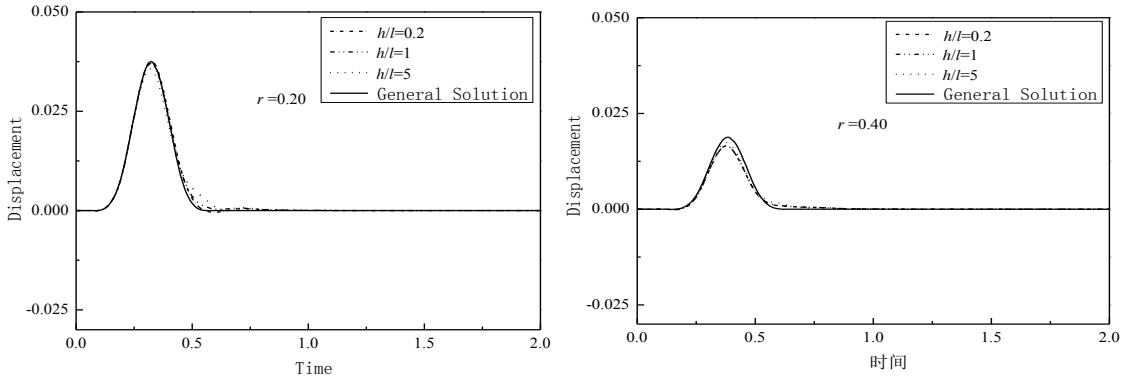

(a) r=0.20 (b) r=0.40

Fig. 7. Results with different sizes of boundary element

Layered half-space infinite problem The 3D model size is 2×2×1. The density of medium is 1. It is divided into two layers. The c_s and ν of the upper layer are 2 and 0.3, respectively. The c_s and ν of the bottom layer are 4 and 0.25, respectively. The range of the uniform load p(t) is $0.5 \quad x,y \quad 0.5$, and the loading duration is 1.0s. The other parameters are the same as the values defined in the above example.

The displacement of the observed point along the z direction is shown in Fig. 8. The theory solution is the expanded solution obtained by the FEA. The 3D equivalent boundary element has the same accuracy and stability as the lumped viscous-spring artificial boundary model. The robust of the parameter h is studied in Fig. 9. The results show that the size of the 3D equivalent boundary element has little effect on the results.

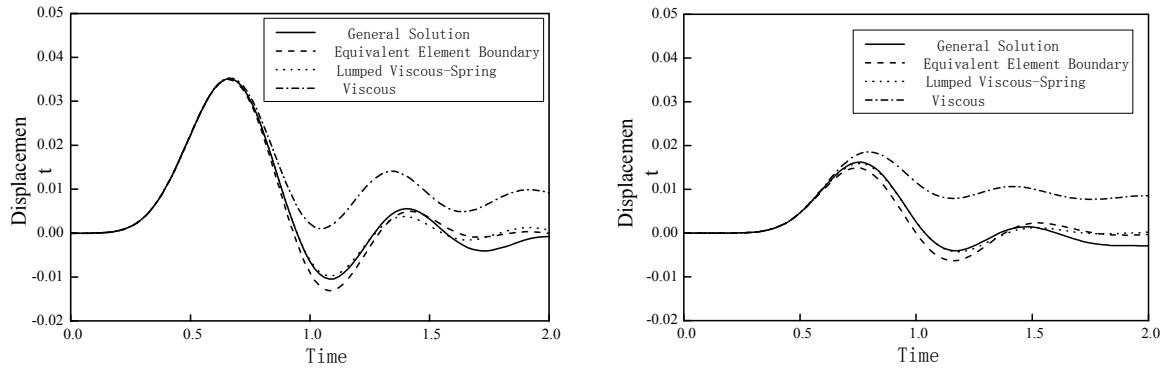

(a) A(0.5, 0.0, 0.0) (b) B(0.5, 0.0, 0.5)

Fig. 8. The time history of displacements for observe point

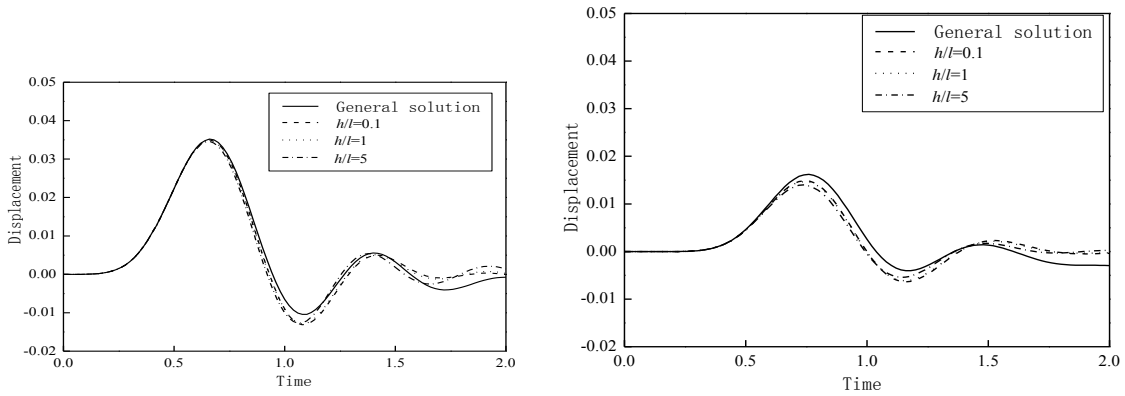

(a) A(0.5, 0.0, 0.0) (b) B(0.5, 0.0, 0.5)

Fig. 9. Results for the layered half-space problem with different h/l

From the study above, the equivalent boundary method has the same accuracy with the original spring-damper system. It is convenient that the thickness of the equivalent artificial boundary element can be changed on a large scale.

3. INPUT SEISMIC WAVES WITH OBLIQUE INCIDENCE

3.1 Input seismic waves

P waves and SV waves can be interchanged when they pass through the boundary of different mediums. Waves of oblique incidence produce P and SV waves and their reflected waves are shown in Fig.10.

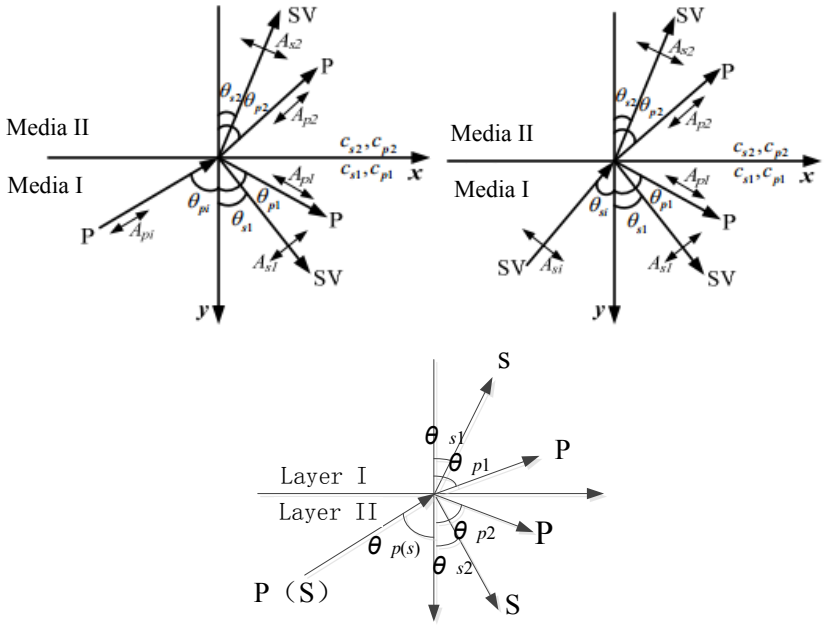

Fig.10. Sketch of oblique incidence propagation

Let the horizontal direction as the x-axis and vertical direction as y-axis. There is an angle, θ, between the motion direction and y-axis. The apparent wave velocity along horizontal direction is shown in Eq. (19),

$$c_x = \frac{c_{p1}}{\sin\theta_{pi}} \tag{19}$$

in which c_x is the horizontal apparent wave velocity and c_{p1} is the propagation velocity in a medium of layer 1. According to the Snell rule, the shear velocity in the horizontal direction in each soil layer is the same. The horizontal velocities of seismic waves have the following relation,

$$\frac{c_{s1}}{\sin\theta_{s1}} = \frac{c_{p1}}{\sin\theta_{p1}} = \frac{c_{s2}}{\sin\theta_{s2}} = \frac{c_{p2}}{\sin\theta_{p2}} \quad c_x \tag{20}$$

in which c_{s1} is the velocity of the S wave propagating in layer 1. c_{p1} is the velocity of the P wave propagating in layer 1. c_{s2} is the velocity of S wave propagating in layer 2. c_{p2} is the velocity of the P wave propagating in layer 2.

Considering the effect of traveling wave, when the P wave propagates in oblique incidence, the displacement in the free field can be written in Eq. (21) in the elastic medium of the layer.

$$u(x,y,t) = u(0,y,t-\frac{x}{c_x}) \tag{21}$$

Substitute t as Δt (time step), the equation can be written as

$$u(jc_x\Delta t, y, t) = u(0, y, t - j\Delta t) \tag{22}$$

The free fields response of an half space subjected to oblique incidence can be calculated by the time history method of one dimension[0]. According to the wave motion in Eq. (22), displacements of left, right and bottom boundaries can be calculated. The finite element method of lumping mass, which means the motion of any node is only related to the neighboring nodes, is used to calculate the time-history force in the three faces of the boundaries. Considering the accuracy and stable of the numerical solution, this method should meet the following condition: $\Delta t <= \frac{\Delta y}{c_s}$ in S wave and $\Delta t <= \frac{\Delta y}{c_p}$ in P wave.

According to the method mentioned above, the problem of the seismic wave propagation is transferred to the problem of the wave source. A program of adding equivalent loading on the artificial boundaries is made by MATLAB software. The angle, θ can be set to 0 when neglecting oblique incidence. The procedure is shown in Fig. 11.

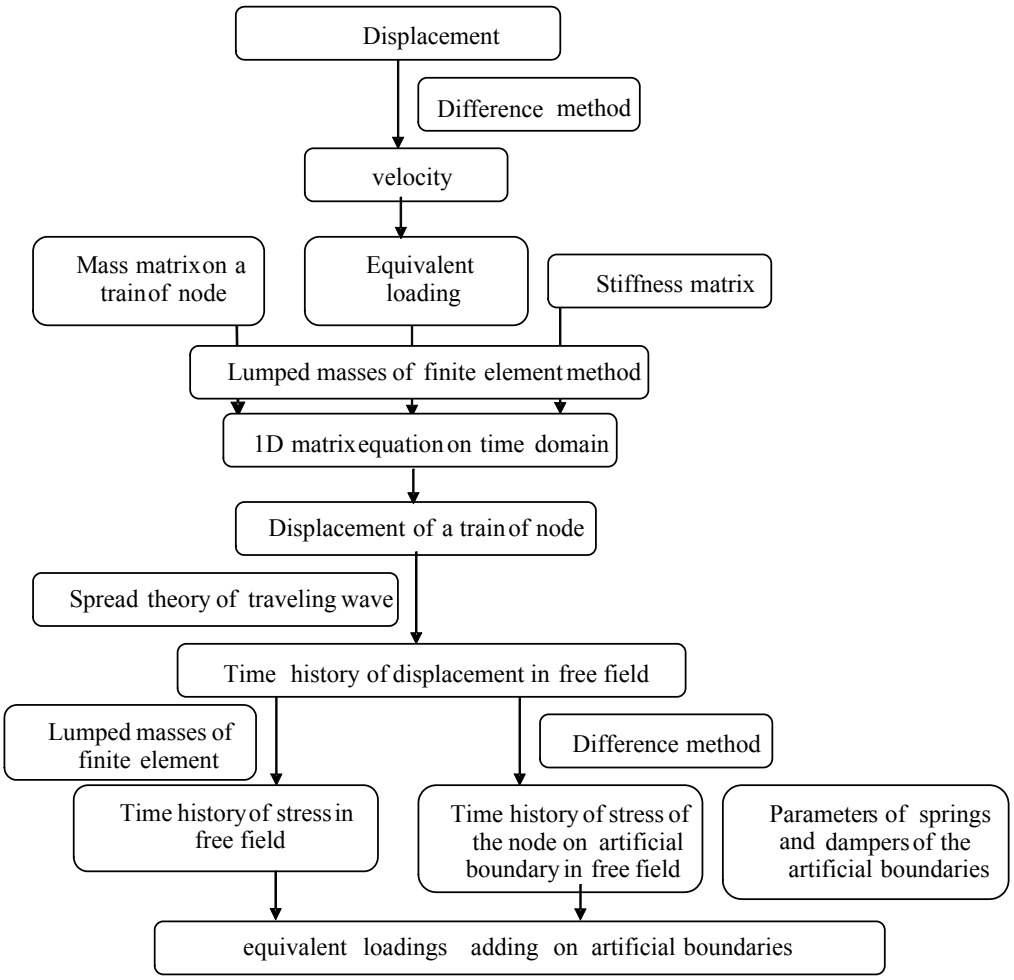

Fig.11 Flowchart of solution for the equivalent load on the node of artificial boundary

3.2 Verification of the procedure

A model of layered media, as the example used in reference [Wang, 2007], is selected for testing the accuracy of the method. A layer of artificial boundaries is set on the left, right and bottom sides of the free field. The equivalent loading is added on each node of the boundary in both x and y directions. A sketch of the model is shown in Fig.12(a). The displacement time history of the input curve for point B is shown in Fig.12(b). The parameters of the soil

are shown in Table 1.

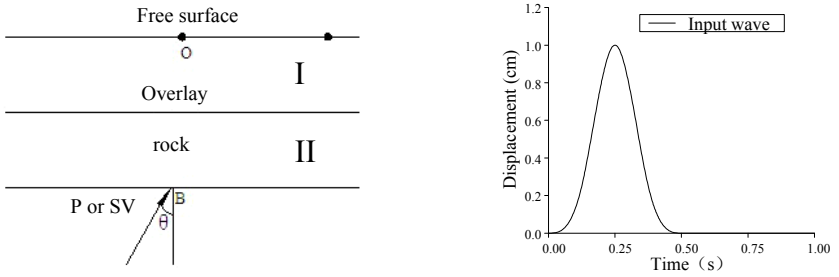

(a) Location of the Input wave (b)Time history curve of input wave

Fig. 12 Sketch of the model and the input wave

s	Thickness（m）	Density（Kg/m^3）	V_s（m/s）	V_p（m/s）
I	50	1000	200	346
II	50	1500	500	866

Table 1 Parameters of the soil

The results shown in Fig.13 are close to the results in reference [Wang,2007], which showed as u_x and u_y in Fig. 13. The results validate the input method proposed.

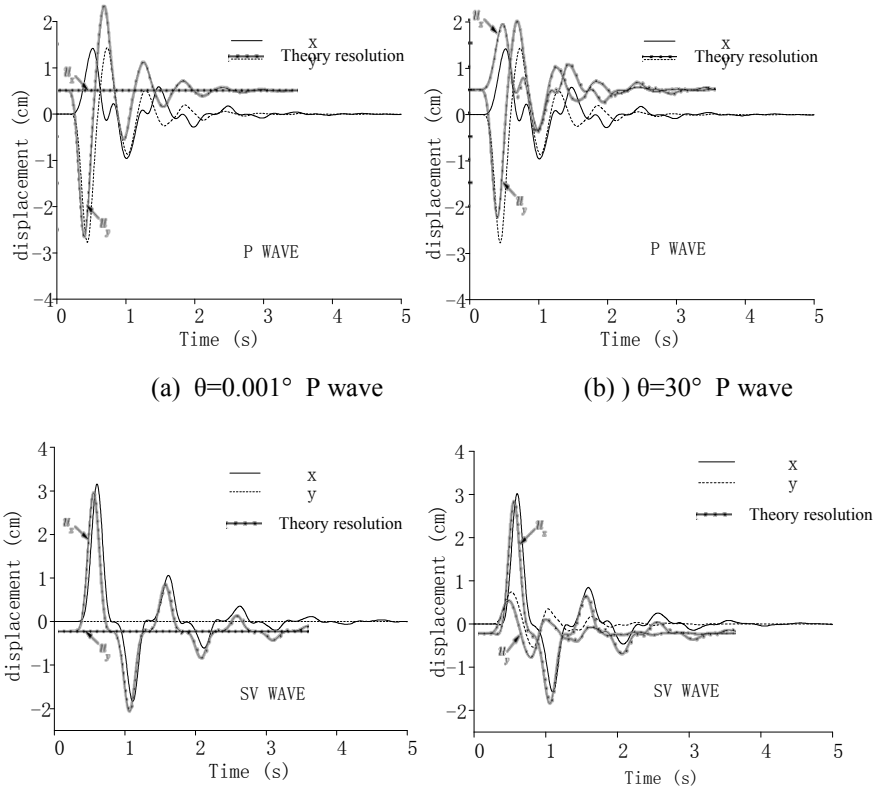

(a) θ=0.001° P wave (b)) θ=30° P wave

(c) θ=0.001° SV wave (d) θ=30° SV wave

Fig.13. Time history curves of displacement with different angles

4. CASE STUDY 1: APPLICATION TO PLAIN OBLIGUE AND NON-OBLIGUE CASES

4.1 The plain non-obligue case

A numerical model was built of a continuous rigid bridge with the total length of 560m and its spans of 100m+180m+180m+100m. The pier is a RC double wall of 2 m thickness, 9.0 m depth, and about 30 meters height. The diameter of the circle pile is 2.8m with length of 20m . The main features and the basic dimensions of the bridge are shown in Fig.14(a). The numerical model of the bridge-structure system is shown in Fig.14(b). The parameters of the model elements and soils are shown in Tables 2 and 3, respectively. The longitudinal direction along the bridge is ordinates x, perpendicular to which is transverse direction of ordinates y and vertical direction of ordinate z.

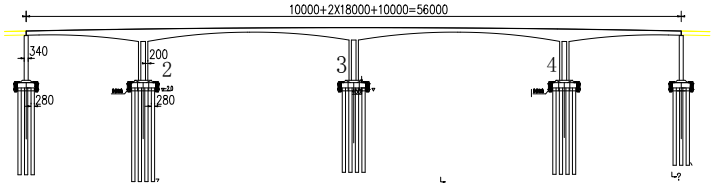

(a) Elevation

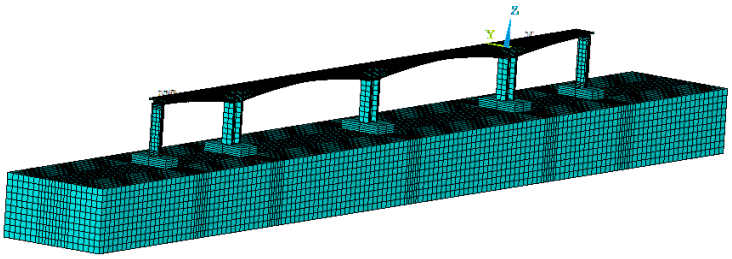

(b) Soil-bridge finite element model

Fig.14. Layout of the long-span bridge and FEA model

Type of Elements	BEAM188	MASS21	SOLID45	BEAM4
Component of Structures	Girder, pier, pile	Lump mass	Soil	Rigid

Table 2 FEA model and element

No.	V_S (m/s)	V_P (m/s)	μ	P (kg/m3)	Thickness (m)
1	350	633.2	0.28	2100	10
2	400	723.6	0.28	2100	10
3	500	866	0.25	2200	30

Table 3 Material parameters of multi-layered soil

4.2 Input seismic wave

Three earthquake waves are selected including Loma Prieta(NS,GMR090), Kobe(NS,JMA) and Qianan(NS, Tianjin Hospital station) accelerogram. The peak ground accelerations of the three waves are scaled to 0.1g. The waves of displacement and acceleration are shown in Fig.15. The earthquake input is considered in the longitudinal direction with wave propagating from left to right. It is shown in Fig.16 that the three waves have different

frequencies. Most of the Kobe waves are within the limits of low frequencies with high frequencies decreasing rapidly. Qianan waves have more high frequency components. The displacements of the spectrum curves are differentiated, as shown in Fig.16(b).

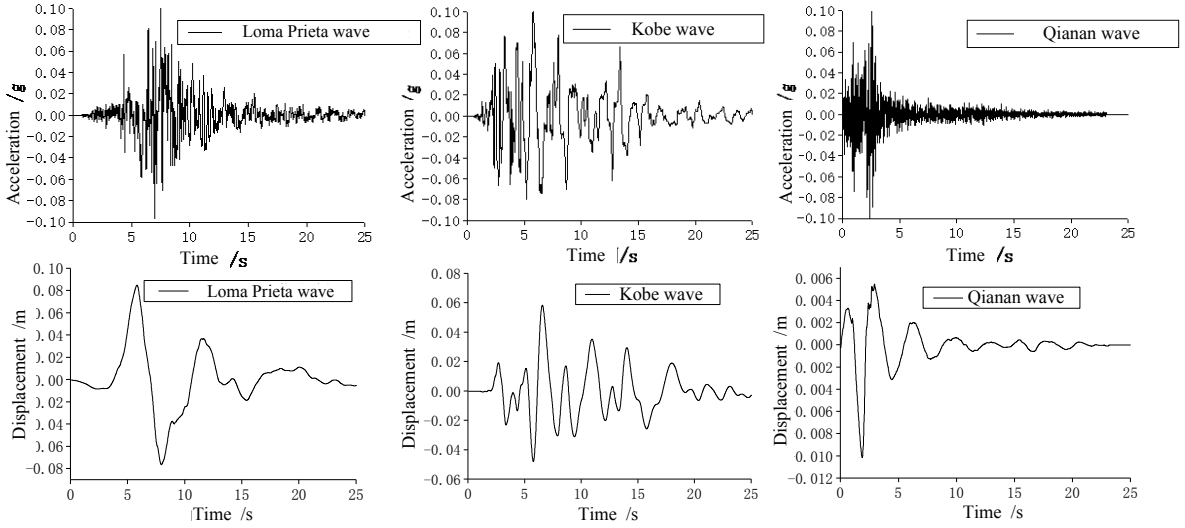

Fig.15. The history curves of acceleration and displacement of the input earthquake waves

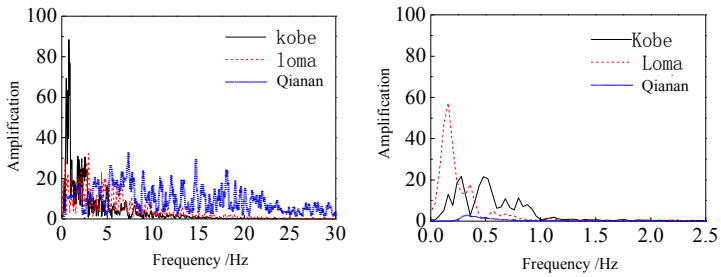

（a）Acceleration （b）Displacement

Fig.16. Fourier spectrum curve of the input waves

4.3 Oscillation characteristics of the local site-bridge system

The open system is turned to a closed system by adding a local artificial boundary condition. The oscillation characteristics of a local site-bridge system are studied. The first five modes of vibration are listed in Table 5. The first vibration mode is longitudinal drift. The first, second and 30th mode of the soil-structure are shown in Fig.17.

Modes	Freqency（Hz）	Shape characteristic	Participation factor
1	0.35619	Longitudinal drift of main girder	7011.0
2	0.71726	Anti-symmetric Transverse bending of main girder	0.0024
3	0.73761	symmetric Transverse bending of main girder	-0.00024
4	0.83761	Anti-symmetric vertical bending of main girder	29.758
5	1.0158	symmetric vertical bending of main girder	0.425

Table 5 Dynamic Characteristic

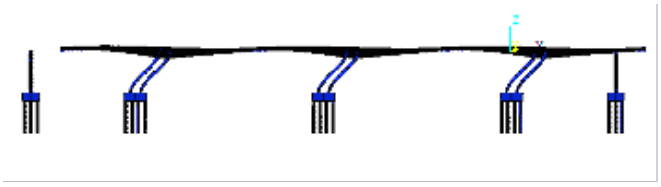

（*a*）1st mode

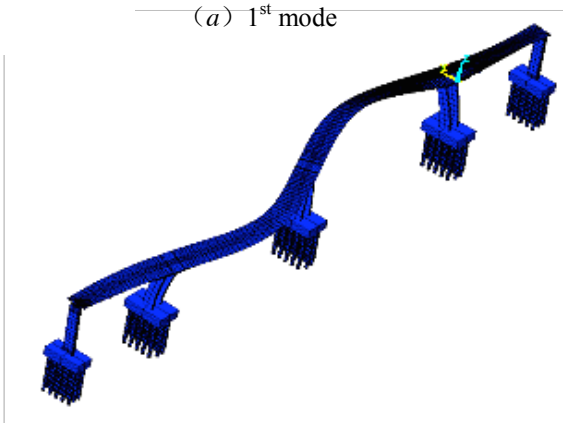

（*b*）2nd mode

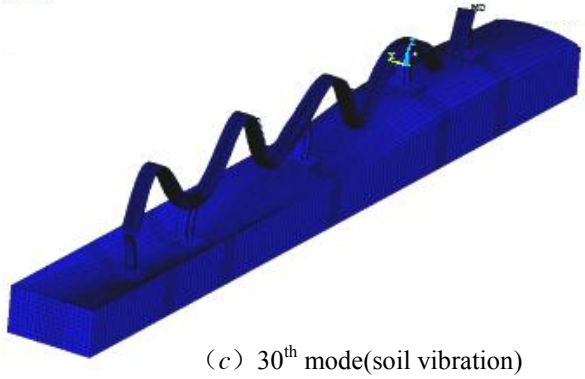

（*c*）30th mode(soil vibration)

Fig.17. Vibration mode of a structure-foundation system

4.4 Response of bridge system subjected to oblique incidence waves case

The bottom and top of the continuous rigid frame bridge are the vulnerable parts under earthquake. The internal forces of the piers are studied below, focusing on bottom of the piers. The number of piers and the location are shown in Fig.14(b).

The three waves travel as P and SV waves are analyzed under different oblique incidence angles. The shear history curves of the 3th pier are shown in Fig.18. The shear forces under P waves are generally smaller than those under SV waves. Moreover, the shear forces increase with increasing angle of incidence for P waves while the effects of angle if incidence is less evident for S wave input.

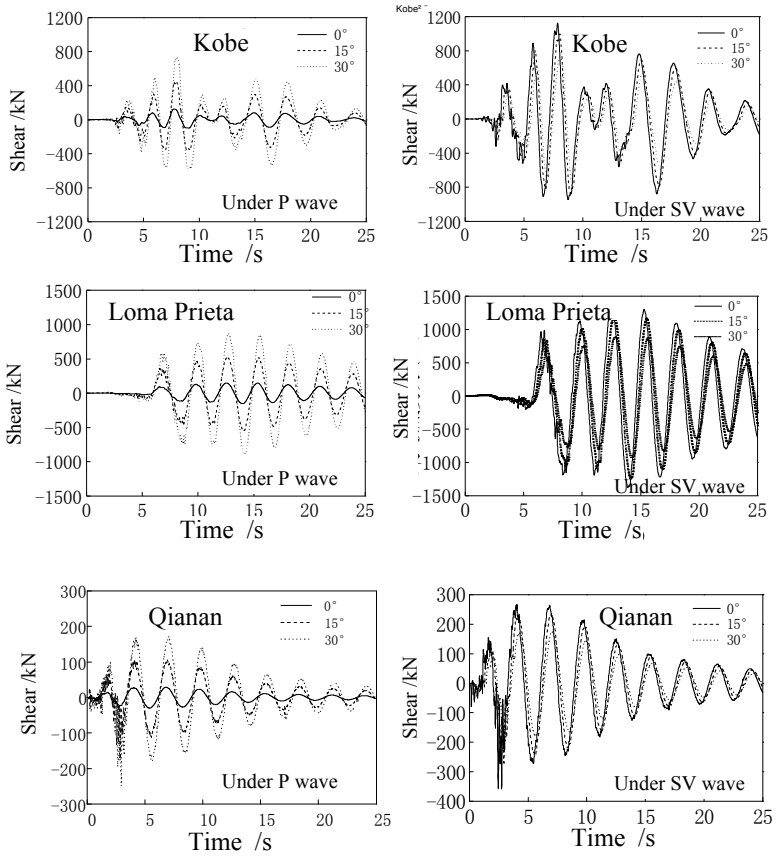

（a）P waves （b）SVwaves

Fig.18. Response history curves of shear forces under three earthquake waves with different angles of incidence

The bending moment and axial forces of three main piers are shown in Figs.19 and 20, respectively. The forces of the piers are not symmetric to the central pier any more when the angle of input of waves is not vertical. The angles of incidence waves differed from affecting the axial force and the bending moments. The bending moments M_y of all three piers increase as angles of P incidence wave increase with the axial forces of some piers increasing. It is not the same rule to the axis forces. The response under P waves is usually smaller than that under SV waves. But the increase is obvious so the effect should be noticed. The figures show a reverse trend to the forces under the SV waves. The bending forces decrease as angles increase. On the contrary, the axial forces of the piers are increased as the angles increase.

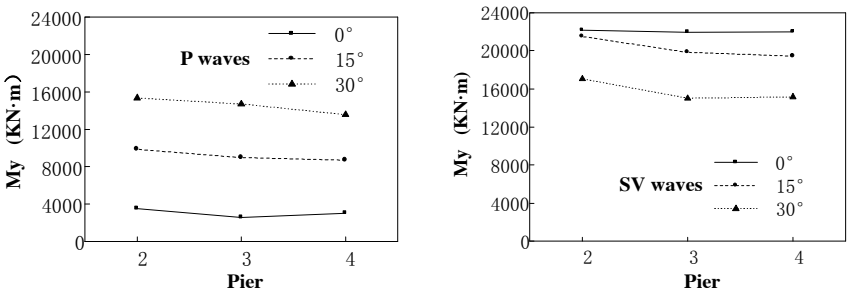

（a）Under Kobe waves

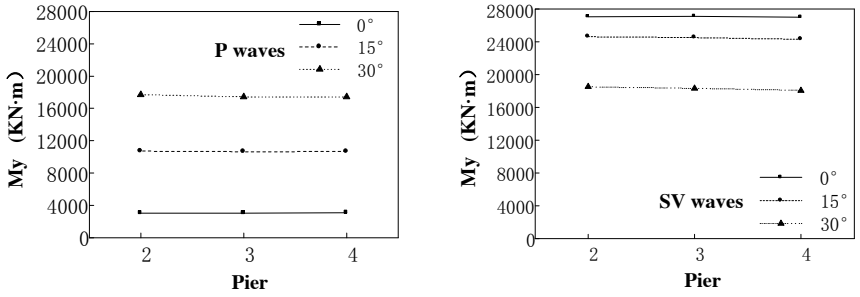

（b）Under Loma Prieta waves

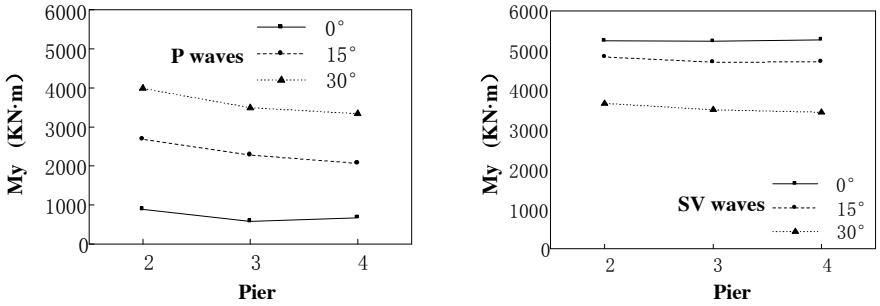

（c）Under Qianan waves

Fig.19. Maximum amplitude of bending moment under three earthquake waves with different angles of incidence

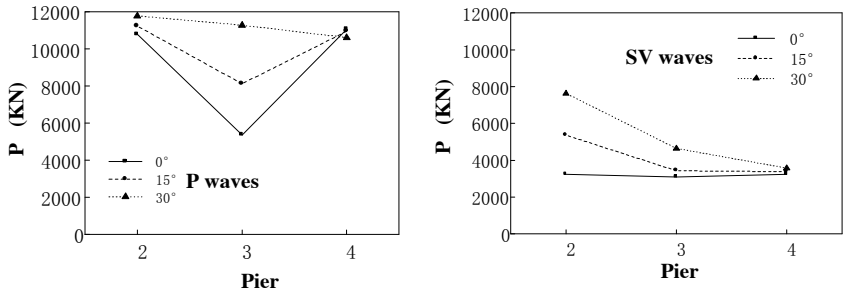

（a） Under Kobe waves

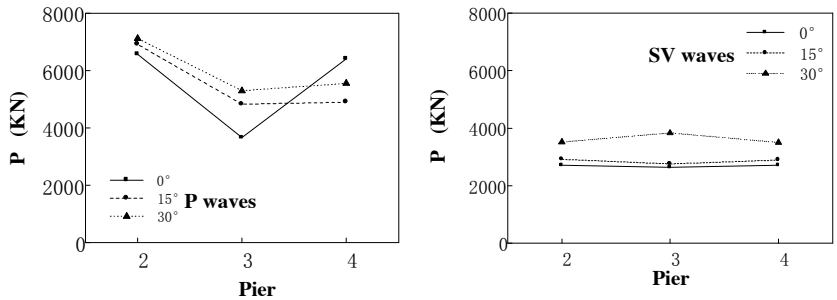

(b) Under Loma Prieta waves

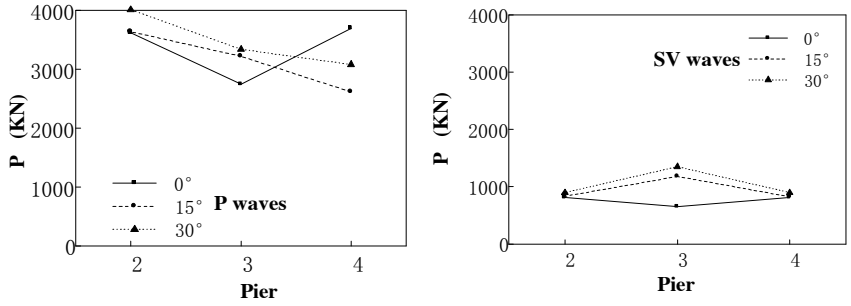

（c）Under Qianan waves

Fig.20. Maximum amplitude of axial forces under three earthquake waves with different angles of incidence

5. CASE STUDY 2: THE TOPOGRAPHIC SHAPE OBLIGUE CASE

5.1 Case study model

The finite element model with the same bridge shown in Fig.14 and non-horizontal soil profile is shown in Fig.21.

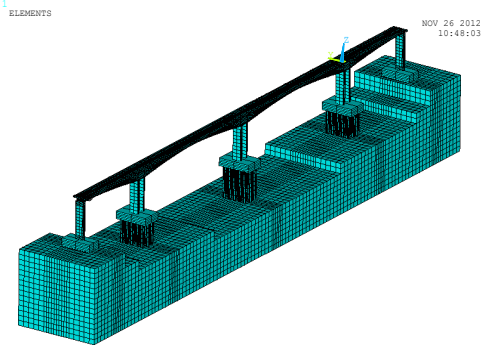

Fig.21 The numerical model of bridge with special topographic shape

5.2 Input seismic wave

We selected the Anza Earthquake record that has a short duration to reduce the time for computing. The time history curves of acceleration and displacement are shown in Fig.22. The peak of the displacement is 0.16cm. The time step is 0.004s.

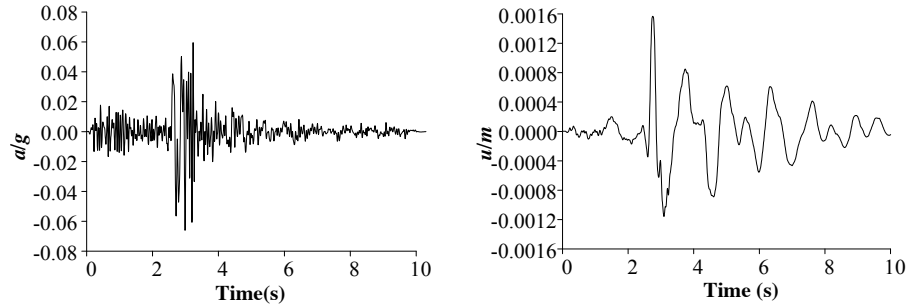

（a）Acceleration　　（b）Displacement

Fig.22. Input earthquake wave

5.3 Results and discussion

The results of the internal forces are compared for vertical and oblique incidence of input waves. The bottom and the top of the pier are the most vulnerable locations in this rigid continuous bridge. The force at the bottom is larger than that at the top in this case. So the internal forces at the top of piers are studied. The locations of the numbered piers are shown in Fig.14(a). The amplitudes of the internal forces of the piers subjected to P waves of different input angles of the oblique incidence wave are shown in Fig.23. The results show that the shear force of the middle pier is smaller than the other two piers. The shear force and moment of the piers with seismic wave in the vertical direction are smaller than the force and moment with wave characterized by angle of incidence of 30 degree. Conversely, the axial force of the piers is larger for vertical incidence.

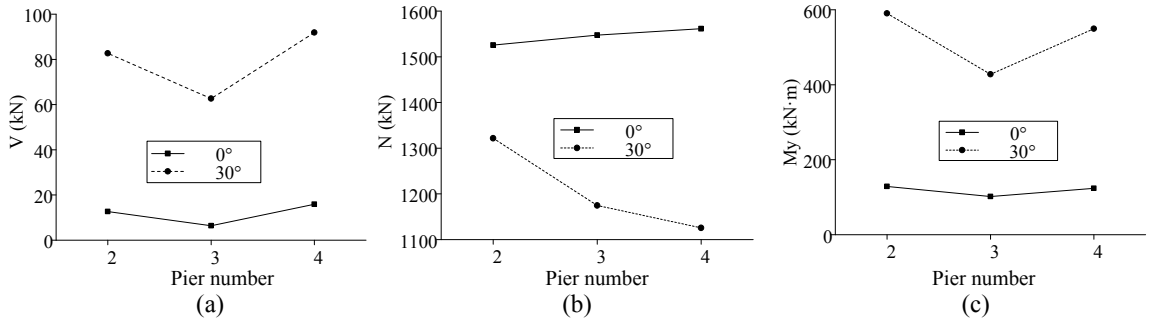

(a) Shear force V (b) Axial force N (c) Moment My

Fig.23. Maximum amplitude of internal forces at bottom of piers under oblique incidence P waves

The amplitudes of the internal forces of piers with SV waves of different input angles of the oblique incidence waves are shown in Fig.24. The shear force of the middle pier is smaller than those of the other two piers as well. But the results of the SV waves show a reverse trend from the P waves. The shear force and moment of the piers with a seismic wave in the vertical direction are larger than the force and moment with wave characterized by angle of incidence of 30 degrees. Conversely, the axial force of the piers is smaller for vertical incidence.

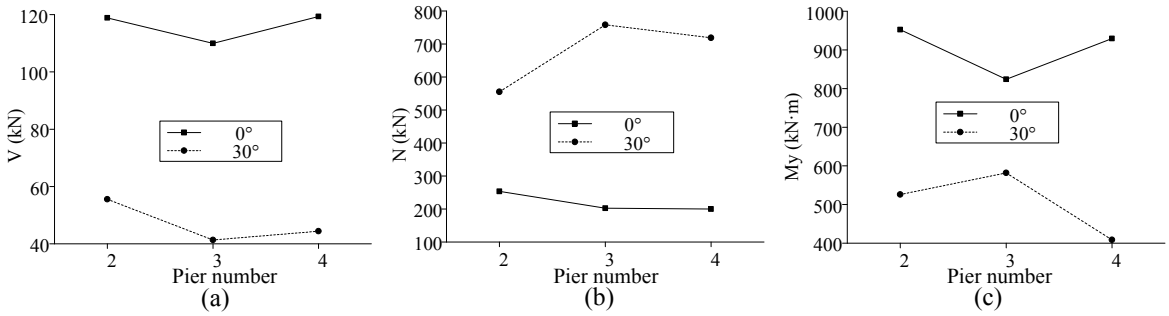

(a) Shear force V (b) Axial force N (c) Moment My

Fig.24. Maximum amplitude of internal forces at bottom of piers under oblique incidence SV waves

Considering ratio of the values computed from the vertical and oblique incidence input, an index can be calculated as follows:

$$\eta = \frac{\max|F| - \max|F_0|}{\max|F_0|} \tag{23}$$

in which F_0 is the internal force of the piers including shear forces, axial forces and moment computed by vertical input; F is the internal force computed by an oblique incidence wave.

The indices of non-uniform effects for piers in a valley under oblique incidence waves at 30 degrees are shown in Table 6. It is shown that the oblique incidence waves have a great effect on the piers of bridges in the valley.

Internal forces	η_P			η_{SV}		
	Pier 2	Pier 3	Pier 4	Pier 2	Pier 3	Pier 4
V	552%	874%	477%	-53.28%	-62.39%	-62.80%
N	-13%	-24%	-27%	118.86%	274.26%	259.41%
M_y	359%	319%	344%	-44.76%	-29.41%	-56.02%

Table 6 Indices of non-uniform effects for piers of a valley under oblique incidence waves at 30 degrees

6 CONCLUSIONS

This study is focused on building a simple model of bridge-soil dynamic interaction considering the effect of oblique incidence waves. The three-dimensional equivalent viscoelastic boundary element is introduced based on the theory of viscoelastic artificial boundary. The open system is turned to a closed system using local artificial boundary. A seismic inputting procedure of oblique incidence waves is proposed by adding equivalent loading on the artificial boundaries. The seismic analysis of a continuous rigid frame long-span bridge was studied under oblique incidence waves. The amplitude and distribution of internal forces of piers were studied. The influencing factors including seismic waves input, oblique incident angle and shear wave velocity of the soil were analyzed.

The input angles have different effects on the dynamic response of continuous rigid frame bridges under P-wave and SV-waves.The results show that the shear force and moment of the piers under P waves in the vertical direction are smaller than the force and moment with inputting waves at a 30 degree angle. The axial force of the piers is larger in the vertical direction. For the seismic SV waves, on the contrary, the shear force and moment of the piers under wave in the vertical direction are larger than the force and moment with inputting waves at a 30 degree angle. The axial force of the piers is smaller in the vertical direction. It is shown that the oblique incidence has great effects on the long-span bridges with high piers, and affects bridges in a valley.

REFERENCES

[1]. Alys, N. and Ahmed, M. A, Effect of ground motion spatial variability on the response of cable- stayed bridges. *Earthquake Engineering Structural Dynamics*, **21**, 1-20, 1992.

[2]. Ariane Ducellier, Hideo Aochi, Interactions between topographic irregularities and seismic ground motion investigated using a hybrid FD-FE method. *Bull Earthquake Engineering*, **10**, 773–792, 2012.

[3]. Bonganoff, J. L., Goldberg, J. E., Schiff, A. J, The effect of ground transmission time on the response of long structures. *Bull Seism Soc Am*, **55**, 627-640, 1965.

[4]. Chen W. [2007] "Seismic response analysis of underground structures under obliquely incident seismic waves," Master dissertation, Beijing University of Technology, Beijing, China. (In Chinese)

[5]. Deeks, A. J., Randolph, M. F, Axisymmetric Time-domain Transmitting Bondaries. *Journal of Engineering Mechanics* , **120**(1), 25-42, 1994.

[6]. Du, X. L., Chen, W., Li, L., and Li, L. Y, Preliminary study of time-domain seismic response for underground structures to obliquely incident seismic waves. *Technology for Earthquake Disaster Prevention* , **2**(3), 290-296, 2007.

[7]. EN, *Eurocode 8: Structures in seismic regions design*. Brussels European Committee for Standardization. 1995.

[8]. Gaffet, S., Bouchon, M, Effects of two-dimentional topographies using the discrete wavenumber-boundary integral equation method in P-SV cases *J*. *Acoust*. *Soc*. *Am*, **85**, 2277-2283, 1989.

[9]. Gu, Y. [2005] "Theoretical Analysis of the Efficient Numerical method for Soil-Structure Dynamic Interaction and its Application," Ph.D. dissertation, Tsinghua University, Beijing, China. (In Chinese)

[10]. Gu, Y., Liu, J. B., Du, Y. X. [2007] "3D Consistent viscous-spring artificial boundary and viscous-spring boundary element," *Engineering Mechanics* **24** (12), 31-38 (In Chinese)

[11]. JTG/TB 02-01-2008. [2008] *The Rules of seismic design for highway bridges*. The Department of Transportation. People's Communication Press, Beijing, China. (In Chinese)

[12]. Li, B. [2005] "Theoretical Analysis of Seismic Response of Underground Subway Structures and Its Application," Ph.D. dissertation, Tsinghua University, Beijing, China. (In Chinese)

[13]. Liu, B. D., Zhou, Zh. H., Liu, P. X., Li, X. J., Wang, W. [2011] "Influence of V-shaped canyon site on ground motions for incident SV waves," *Earthquake Engineering and Engineering Vibration* **31**(2), 17-25.(In Chinese)

[14]. Liu, J. B., Wang, Zh. Y., Du, X. L., Du, Y. X. [2005] "Three Dimensional viscous-spring artificial boundaries in time domain for wave motion problems," *Engineering Mechanics* **22**(6), 46-51. (In Chinese)

[15]. Liu Lin. [2005] "Random vibration analysis of bridges considering topographic effects," Ph.D. dissertation, Beijing University of Technology, Beijing, China. (In Chinese)

[16]. Lysmer, J. and Kulemeyer, R. L, Finite Dynamic Model for Infinite Media, Journal of Engineering Mechanics. *Journal of the Engineering Mechanics Division. ASCE* **95**, 759-877, 1969.

[17]. Paolucci, R, Amplification of earthquake ground motion by steep topographic irregularities. *Earthquake Engineering Structural Dynamics* **31**, 1831–1853, 2002.

[18]. Sun, L. M., Zhang, Ch. N., Pan, L. [2002] "Lumped-mass model and its parameters for dynamic analysis of bridge pier-pile-soil system," *Chinese Journal of Tongji University* **30**(4), 409-415. (In Chinese)

[19]. Trifunac, M. D, Scattering of plane SH waves by a semi-cylindrical canyon. *Earthquake Engineering Structural Dynamics*, pp. 1-267, 1973.

[20]. Wang, Q., Chen, J., Li, J, Seismic response analysis of underground pipeline under obliquely incident seismic waves. *Journal of Huazhong University of Science and Technology* **25**(4), 283-286, 2008.

[21]. Wang, Y. [2007] "Research on the Numerical Method for Asynchronous Seismic Wave Motions and its Application in Dynamic Analysis of Structures," Ph.D. dissertation, Tsinghua University, Beijing, China. (In Chinese)

[22]. Zhang, J., Nicos, M, *Seismic Response Analysis of Highway Overcrossings Including Soil-Structure Interaction*, PEER Report, University of California, Berkeley, 2001.

[23]. Zhang, N., Gao, Y. F., Li, D. Y., Wu, Y. X. and Zhang, F, Scattering of SH waves

induced by a symmetrical V-shaped canyon: a unified analytical solution. *Earthquake Engineering and Engineering Vibration* **11**, 445-460, 2012.

[24]. Zhou, G. L. [2010] "Canyon topography effects on seismic response of multi-support bridges," Harbin: Institute of Engineering Mechanics, China Earthquake Administration. (In Chinese)